Cramér-Rao Bounds for Parametric Shape Estimation in Inverse Problems

Jong Chul Ye, Yoram Bresler and Pierre Moulin

Abstract— **We address the problem of computing fundamental performance bounds for estimation of object boundaries from noisy measurements in inverse problems, when the boundaries are parameterized by a finite number of unknown variables. Our model applies to multiple unknown objects, each with its own unknown gray level, or color, and boundary parameterization, on an arbitrary known background. While such fundamental bounds on the performance of shape estimation algorithms can in principle be derived from the Cramér-Rao lower bounds, very few results have been reported due to the difficulty of computing the derivatives of a functional with respect to shape deformation. In this paper, we provide a general formula for computing Cramér-Rao lower bounds in inverse problems where the observations are related to the object by a general linear transform, followed by a possibly nonlinear and noisy measurement system.**

I. Introduction

THE problem of estimating object boundaries from noisy measurements is encountered in applications such as computed tomography (CT), image deconvolution, synthetic aperture radar (SAR), and nonlinear inverse scattering.

In such problems, the boundary is often parameterized by a finite number of unknown variables. Such a parametric formulation (for instance using B-splines [1] or Fourier descriptors [2]) is a first step towards constructing a stable boundary estimation algorithm. Once a suitable parametric model has been identified, fundamental bounds on the performance of shape estimation algorithms can in principle be derived by computing the Cramér-Rao lower bound (CRB).

Cramér-Rao lower bounds are widely used in problems where the exact minimum-mean-square error of an estimator is difficult to evaluate. While CRB's are available for estimation of signal parameters such as direction-of-arrival (DOA) [3], and size and orientation of a scatterer [4], only recently has this type of analysis been conducted for estimation of target shapes [5, 6]. In [5], the boundary of a star-like target is parameterized using B-splines, and CRB's for the B-spline coefficients are computed for several shapes in a magnetic resonance imaging problem. However, the results in [5] are applicable only to star-shaped objects.

For nonlinear inverse scattering problems, Ye, Bresler and Moulin [6] employed the domain derivative to compute the CRB for arbitrarily shaped objects. The main goal of this paper is, therefore, to extend the domain derivative idea of [6] to compute CRBs for shape estimation for general linear inverse problems. The techniques and results developed in this paper therefore have broad applicability in imaging problems.

The CRB's computed using the techniques of this paper can also be used to compute a global uncertainty region around the boundary [7], providing an easily interpreted geometric display of boundary uncertainty. A related idea has been applied to tomographic reconstruction by Hanson *et al* [8]. The uncertainty regions in [8] were however constructed using Monte-Carlo simulations for a particular estimator. Hence, they are limited to that estimator, and are time-consuming to construct. In contrast, our global confidence region can be easily and quickly constructed using the CRB covariance matrix, even before the construction of an estimator is attempted.

J.C. Ye is now with Philips Research, Briarcliff Manor, NY 10510. Email: Jong.Ye@philips.com.

Y. Bresler and P. Moulin are with the Coordinated Science Laboratory, Department of Electrical and Computer Engineering, University of Illinois at Urbana-Champaign, 1308 W. Main Street, Urbana, IL 61801. Email: {yoram,moulin}@ifp.uiuc.edu

This work was supported by a grant from DARPA under Contract F49620-98-1-0498, administered by AFOSR, and by NSF Infrastructure Grant CDA 96-24396.

II. The Shape Estimation Problem

Consider a real-valued image f consisting of a constant-valued 2-D object and a known background density $f_2(x, y)$:

$$f(x,y) = \begin{cases} f_1, & (x,y) \in D \\ f_2(x,y), & (x,y) \in \mathbb{R}^2 \backslash D \end{cases} . \quad (1)$$

The intensity f_1 and region D are unknown, whereas $f_2(x, y)$ is known for all $(x, y) \in \mathbb{R}^2$. This scenario models an object of constant but unknown intensity and unknown shape, partly occluding (or replacing) a known background. The object is thus completely defined by its density f_1 and its boundary $\Gamma = \partial D$. The support set D need not be a connected region, so the formulation includes the case of multiple objects. Let $g = \mathcal{H}f$ be a general linear integral transformation of f, defined by

$$g(s,t) = \int_{-\infty}^{\infty}\int_{-\infty}^{\infty} f(x,y)h(x,y,s,t)dxdy \ , \quad (s,t) \in \Omega \quad (2)$$

where $h : \mathbb{R}^2 \times \Omega \to \mathbb{R}$ is a known kernel, and Ω a subset of $\mathbb{R}^2$. Suppose $g(s, t)$ is sampled at a finite number M of positions $\{s_m, t_m\}_{m=1}^M$.

The estimation problem we consider is to estimate the object boundary Γ from noisy measurements $\{y_m\}_{m=1}^M$ of the samples $g_m = g(s_m, t_m)$, $m = 1, \cdots, M$. Our goal is to derive fundamental bounds on the estimation accuracy of Γ for specified statistics of the measurement noise.

For each imaging modality, the operator kernel $h(x, y, s, t)$ varies. For example, in a computed tomography problem, Eq. (2) becomes a 2-D Radon transform with a kernel $h(x, y, s, t) = \delta(x\cos(s) + y\sin(s) - t)$, while in a Fourier imaging problem the kernel becomes $h(x, y, s, t) = e^{-j2\pi(sx+ty)}$.

III. Statistical Framework for Parametric Shape Estimation

A. Parametric Boundary Model

The boundary function Γ lives in an infinite-dimensional space, and thus the estimation of Γ from a finite number of noisy samples $\{y_m\}_{m=1}^M$ is generally an ill-posed inverse problem. A possible remedy is to represent the boundary Γ as a known function with a finite number of unknown parameters:

$$\Gamma \quad = \quad \{\boldsymbol{\zeta}(u;\boldsymbol{\phi}), u \in I\} \ , \quad (3)$$

where $\boldsymbol{\phi} = (\phi_1, \cdots, \phi_K) \in \mathbb{R}^K$ is an unknown parameter vector, and $I \subset \mathbb{R}$ an interval. In particular, we use the series expansion model

$$\boldsymbol{\zeta}(u;\boldsymbol{\phi}) = \big[x(u;\boldsymbol{\phi}), \quad y(u;\boldsymbol{\phi})\big]^T = \sum_{i=1}^{K} \phi_i \mathbf{b}_i(u) \quad , \quad u \in I \ , (4)$$

where $\mathbf{b}_i(u) \in \mathbb{R}^2$ is the i-th basis function. Parameterizations such as B-splines [1] and Fourier descriptors (FD) [2] are special cases of this model and have been widely used for shape representation. Throughout the paper, we denote the m-th noise-free sample $g(s_m, t_m)$ by $g_m = g_m(\boldsymbol{\theta})$, where $\boldsymbol{\theta} = [f_1, \phi_1, \cdots, \phi_K]^T$.

B. The Cramér-Rao Inequality

The measurements $\mathbf{y} = \{y_m\}_{m=1}^M$ are a noisy version of $\mathbf{g} = \{g_m\}_{m=1}^M$. The measurement model is specified by a conditional probability density function (pdf) $p_{Y|\mathbf{g}}(\mathbf{y}|\mathbf{g}) = p(\mathbf{y}|\boldsymbol{\theta})$, where $\mathbf{y}$ denotes a particular realization of the random vector Y. Note that this formulation includes the case where the observation involves a nonlinear transformation of $\mathbf{g}(\boldsymbol{\theta})$. According to the Cramér-Rao inequality, subject to some regularity conditions on the conditional pdf $p_{Y|\boldsymbol{\theta}}$, the $K \times K$ covariance matrix of the estimation error $\hat{\boldsymbol{\theta}} - \boldsymbol{\theta}$ for the unknown parameter $\boldsymbol{\theta}$ is bounded from below as [9]

$$\mathrm{Cov}\left(\hat{\boldsymbol{\theta}} - \boldsymbol{\theta}\right) \quad \geq \quad \mathbf{C}_{\boldsymbol{\theta}} \stackrel{\triangle}{=} (\mathbb{I}_{\boldsymbol{\theta}})^{-1} \ , \tag{5}$$

for *any unbiased* estimate $\hat{\boldsymbol{\theta}}$ of $\boldsymbol{\theta}$, where the Fisher information matrix, $\mathbb{I}_{\boldsymbol{\theta}}$, is the $K \times K$ matrix

$$\mathbb{I}_{\boldsymbol{\theta}} \quad = \quad E\left[\nabla_{\boldsymbol{\theta}} \ln p(\mathbf{y}|\boldsymbol{\theta}) \nabla_{\boldsymbol{\theta}}^T \ln p(\mathbf{y}|\boldsymbol{\theta})\right] \tag{6}$$

where $\ln p(\mathbf{y}|\boldsymbol{\theta})$ denotes the log-likelihood function.

For any pdf $p(\mathbf{y}|\boldsymbol{\theta})$ for which the Fisher information matrix is well-defined, it follows from the chain rule that the entries of $\mathbb{I}_{\boldsymbol{\theta}}$ in (6) are (possibly nonlinear) functions of $g_m(\boldsymbol{\theta})$ and the derivatives $\frac{\partial g_m(\boldsymbol{\theta})}{\partial \theta_i}, i = 1, \cdots, K, \ m = 1, \cdots, M$.

While Eq. (6) looks simple, the actual computation of the CRB is difficult because the techniques for computing the derivatives $\left\{\frac{\partial g_m(\boldsymbol{\theta})}{\partial \theta_i}\right\}$ for models of the form (2) and (3)-(4) have not been studied in the literature, except for the case of a single star-shaped object in a magnetic resonance imaging problem [5]. We now develop a general technique to compute those quantities in a generic linear inverse problem.

C. From CRB's to Global Confidence Regions

In practice, because $\boldsymbol{\zeta}(u; \boldsymbol{\theta})$ describes the geometry of an object, one is interested in assessing the quality of estimates of $\boldsymbol{\zeta}(u; \boldsymbol{\theta})$ in easily interpreted geometric terms. Rather than the quality of estimates of $\boldsymbol{\theta}$ itself, what is needed is a global quality measure for the entire boundary $\left\{\hat{\boldsymbol{\zeta}}(u; \boldsymbol{\theta}), \forall\ u \in I\right\}$. The CRB $\mathbf{C}_{\boldsymbol{\theta}}$ computed by the techniques of this paper can be used, as described in [7] , to construct small-size *global confidence regions* in the asymptotic regime where the estimate is unbiased, efficient, and Gaussian. Bounds are given in [7] for the probability that the entire boundary estimate lies in the global confidence region. We illustrate the construction of such confidence intervals in the numerical examples.

IV. The Domain Derivative

Combining the object model (1) and the noise-free measurement equation (2) yields

$$\begin{aligned} g(s,t) \quad &= \quad f_1 \int_D h(x,y,s,t) dxdy \\ &+ \quad \int_{\mathbb{R}^2 \setminus D} f_2(x,y) h(x,y,s,t) dxdy \ . \end{aligned} \tag{7}$$

Equation (7) then defines a mapping $J : \{D\} \to \{g\}$ from the set of domains $\{D\}$, or equivalently, boundaries $\{\Gamma\}$, to the space of functions $\{g\}$. This mapping admits the general form:

$$g = J(D) = f_1 \int_D Z_1 dS + \int_{\mathbb{R}^2 \setminus D} Z_2 dS = c + \int_D Z dS \ , \tag{8}$$

where $dS = dxdy$, Z_1, Z_2, and $Z = f_1 Z_1 - Z_2$ are known functions, D is the unknown object support, and $c = \int_{\mathbb{R}^2} Z_2 dS$ is a function independent of D.

The *domain derivative* of this mapping J is the infinitesimal variation of g with respect to an infinitesimal change of boundary Γ [10], and is an essential component of the computation of $\frac{\partial g_m(\boldsymbol{\theta})}{\partial \theta_i}$. Suppose the deformation of the domain can also be given by the deformation of the boundary :

$$\Gamma_t = \Gamma + t\mathbf{q} = \{\mathbf{z} \in \mathbb{R}^N | \mathbf{z} = \mathbf{x} + t\mathbf{q}(\mathbf{x}), \mathbf{x} \in \Gamma\} \ , \tag{9}$$

where the vector field $\mathbf{q} : \Gamma \to \mathbb{R}^N$ is continuously differentiable with respect to arc-length along Γ. For this transformation, we can show the following formula [10]:

$$\delta J(D; q) = \int_\Gamma Z \left\langle \mathbf{q}, \mathbf{n} \right\rangle d\Gamma, \tag{10}$$

where $\mathbf{n}$ denotes the outer-normal vector of Γ.

Note that the derivative of the mapping J of (8) with respect to θ_i is given by the domain derivative of (8) with respect to the following deformation:

$$\Gamma_t = \Gamma + t\mathbf{b}_i = \{\mathbf{z} | \mathbf{z} = \mathbf{x} + t\mathbf{b}_i(\mathbf{x}), \mathbf{x} \in \Gamma\} \tag{11}$$

where $\mathbf{b}_i$ is the i-th basis function in the linear model (4). Therefore,

$$\frac{\partial g}{\partial \theta_i} = \delta J(D; \mathbf{b}_i) = \int_\Gamma Z \left(\mathbf{b}_i^T \mathbf{n}\right) d\Gamma \tag{12}$$

where $\mathbf{b}_i^T \mathbf{n} = < \mathbf{b}_i, \mathbf{n} >$ for notational convenience. The derivative with respect to f_1 is even simpler, of course, because it does not involve the domain derivative: i.e. $\frac{\partial g}{\partial f_1} = \int_D Z_1 dS$.

V. Domain Derivatives for Linear Inverse Problems

A. Connected Boundaries

Because our focus is on the domain derivative technique, we assume in the examples that f_1 is known. Combining Eqs. (1) and (2), we obtain

$$\begin{aligned} g_m(\boldsymbol{\theta}) \quad &= \quad c(s_m, t_m) + \int_D Z(s_m, t_m, x, y) dxdy \\ &\stackrel{\triangle}{=} \quad J(D)(s_m, t_m), \quad 1 \leq m \leq M, \end{aligned} \tag{13}$$

where

$$c(s_m, t_m) \quad = \quad \int_{\mathbb{R}^2} f_2(x,y) h(x,y,s_m,t_m) dxdy \tag{14}$$

$$Z(s_m, t_m, x, y) \quad = \quad (f_1 - f_2(x,y))\, h(x,y,s_m,t_m) \ . \tag{15}$$

Using (12), (13), and (15), we have a 1-D integral formula:

$$\frac{\partial g_m(\boldsymbol{\theta})}{\partial \theta_i} = \int_I \Delta f(u) h\left(x(u), y(u), s_m, t_m\right) \mathbf{b}_i^T(u) \mathbf{n}(u) \tau(u) du \tag{16}$$

$$\Delta f(u) = f_1 - f_2(x(u), y(u)) \tag{17}$$

where $\tau(u)du = d\Gamma$ with $\tau(u) = \sqrt{\dot{x}(u)^2 + \dot{y}(u)^2}$, where $\dot{x}(u)$ and $\dot{y}(u)$ denote the derivatives of x, y with respect to u. In (16), and $\mathbf{n}$ is the outer-normal vector at $(x(u), y(u))$.

An important though somewhat expected observation is the following. Although the measurements, and in fact the existence of the transforms that define them, often depend on all of the background f_2, the Fisher information matrix only depends on the values of the background f_2 on the boundary Γ of the domain D.

B. Partitioned Density

This section extends our previous results to more general image configurations than (1), which assumes f is constant over D. Suppose the image can be partitioned into two disjoint regions,

$$f(x,y) = \begin{cases} f_1(x,y), & (x,y) \in D \\ f_2(x,y), & (x,y) \in \mathbb{R}^2 \backslash D \end{cases} , \tag{18}$$

where the background image $f_2(x,y)$ is known, and the unknown domain D is a union of sub-domains $D_j, j = 1, \cdots, L$:

$$D = \bigcup_{j=1}^{L} D_j \, . \tag{19}$$

Each boundary $\Gamma_j = \partial D_j$ is parameterized as

$$\Gamma_j = \{ \boldsymbol{\zeta}_j(u; \boldsymbol{\theta}_j) : u \in I = [0, 2\pi) \} \, , \tag{20}$$

where $\boldsymbol{\theta}_j \in \mathbb{R}^{K_j}$ denotes a separate unknown parameter vector. Thus, the entire domain D is parameterized by the parameter vector $\boldsymbol{\theta} = [\boldsymbol{\theta}_1^T, \ldots, \boldsymbol{\theta}_K^T]^T$ of dimension $K = \sum_{j=1}^{L} K_j$. In general, the sub-domains D_j need not be disjoint, hence the domain D can be further partitioned into P disjoint regions:

$$D = \bigcup_{k=1}^{P} \Omega_k \quad , \quad \Omega_j \cap \Omega_k = \varnothing, j \neq k \, . \tag{21}$$

Furthermore, for each sub-domain D_j, there exists an index set $Q(j) \subset \{1, \cdots, P\}$ such that $D_j = \bigcup_{k \in Q(j)} \Omega_k$. Figs. 1(a)-(b) give two examples of such disjoint partitions. We require $f_1(x,y)$ to be constant over each set Ω_k:

$$f_1(x,y) = \sum_{k=1}^{P} f_1^k \, \chi_{\Omega_k}(x,y) \tag{22}$$

where χ_{Ω_k} denotes the indicator function of the set Ω_k, and f_1^k is a constant. The partitioned density model (22) is quite general and can also serve an approximation to continuous densities.

Hero *et al* [5] conjectured that to derive performance bounds for the case of multiple domains, detection theoretical analysis using hypothesis testing would be necessary. This problem can however be addressed in an estimation framework. From the partitioned density in (22), we define:

$$f_{1,j}(x,y) = \sum_{k \in Q(j)} f_1^k \chi_{\Omega_k}(x,y) \tag{23}$$

$$f_{1,j^c}(x,y) = \sum_{k \in \{1,\cdots,P\} \backslash Q(j)} f_1^k \chi_{\Omega_k}(x,y) \, . \tag{24}$$

Using (23) and (24), we then have

$$\frac{\partial g(\boldsymbol{\theta})}{\partial \theta_i^{(j)}} = \delta J(D, \mathbf{b}_i^{(j)}) = \int_{\Gamma_j} Z_j \left\langle \mathbf{b}_i^{(j)}, \mathbf{n} \right\rangle d\Gamma \, , \tag{25}$$

where $\theta_i^{(j)}$ and $\mathbf{b}_i^{(j)}$ denote the i-th element of $\boldsymbol{\theta}_j$ and the corresponding basis function, respectively, and

$$Z_j(x,y,s,t) = (f_{1,j}(x,y) - f_{1,j^c}(x,y)) \, h(x,y,s,t) \, . \tag{26}$$

Furthermore, the derivative with respect to the pixel value f_1^k is given by

$$\frac{\partial g(\boldsymbol{\theta})}{\partial f_1^k}(s,t) = \int_{\Omega_k} h(x,y,s,t) dS \tag{27}$$

VI. Numerical Examples

A. Computation of CRB for Connected Boundaries

The motivation for this problem arises from image reconstruction from sparse Fourier samples [11]. Consider the 128×128 MRI scan of a human brain with a tumor in Figure 2(a). The image has 256 gray levels and was taken from a Harvard University medical database [12]. We parameterize the boundary of the tumor using Fourier descriptors (FD) [2]:

$$\begin{aligned} x(u) &= a_0 + \sum_{i=1}^{L} \left(a_i \cos(iu) + a_{L+i} \sin(iu) \right) \\ y(u) &= b_0 + \sum_{i=1}^{L} \left(b_i \cos(iu) + b_{L+i} \sin(iu) \right) \, , \end{aligned} \tag{28}$$

where $L = 15$. In order to overcome the ambiguity due to the starting point of the contour, in (28) the constraint $a_{L+1} = b_1$ is imposed [6]. Hence, the resulting parameter vector $\boldsymbol{\theta}$ is:

$$\boldsymbol{\theta} = \begin{bmatrix} a_0 & a_1 & \cdots & a_{2L} & b_0 & b_2 & \cdots & b_{2L} \end{bmatrix}^T \in \mathbb{R}^{4L+1} \, . \tag{29}$$

The tumor is assumed to have constant intensity.

Suppose that 64 uniformly spaced Fourier samples are taken. This corresponds to $64/(128^2) = 0.4\%$ of the Nyquist sampling rate that would be required to avoid spatial aliasing for this 128×128 image. Suppose furthermore we have a full reference MRI scan of the healthy brain, and know *a priori* the intensity of the tumor, and the number of FD coefficients. Then, the imaging problem can be formulated as shape estimation of the tumor on the known background. Note that in this simulation the known background image has *inhomogeneous* density, and the boundary of the tumor is *not* star-shaped. Using the techniques described in Section V, we calculated the CRB for the unknown FD coefficients.

The CRB matrix $\mathbf{C}_{\boldsymbol{\theta}}$ is 61×61, and even its 61 element diagonal is unwieldy, and their display hard to interpret. Instead we have applied the global confidence region technique of [7] to the example of Figure 2(a) and used the computed $\mathbf{C}_{\boldsymbol{\theta}}$ to compute, in turn, the 98% asymptotic global confidence region, which is readily visualized. Consider an example where the Fourier samples are corrupted with additive complex Gaussian noise with a standard deviation σ equal to 20% of the rms value of the noise-free measurements. (We denote the corresponding signal-to-noise-ratio by SNR=5.) Figure 2(b) illustrates the resulting asymptotic global confidence region, in which asymptotically any unbiased estimate of the boundary will lie with 98% probability. This bound suggests that accurate estimates are possible even at low sampling rates, if we have a parametric description of the tumor shape and know both the density of the tumor and the MRI scan of the healthy brain.

B. Estimating Boundaries of Synthetic Phantom

The motivation of this problem is again image reconstruction from sparse Fourier samples [11]. Consider the 128×128 simulated phantom in Figure 3(a). The phantom consists of four circular boundaries $\Gamma_j, j = 1, \cdots, 4$ (for the disks $D_j, j = 1, \cdots, 4$), which are parameterized by:

$$\boldsymbol{\zeta}_j(u; \boldsymbol{\theta}_j) = \begin{bmatrix} x_j \\ y_j \end{bmatrix} + r_j \begin{bmatrix} \cos(u) \\ \sin(u) \end{bmatrix} \quad , \quad j = 1, \cdots, 4. \tag{30}$$

where $\boldsymbol{\theta}_j = [r_j, x_j, y_j]^T$. The true values of the parameters are given by:

$$\boldsymbol{\theta}_1 = \begin{bmatrix} .80 \\ 0 \\ 0 \end{bmatrix} , \; \boldsymbol{\theta}_2 = \begin{bmatrix} .76 \\ 0 \\ -.02 \end{bmatrix} , \; \boldsymbol{\theta}_3 = \begin{bmatrix} .21 \\ -.20 \\ .35 \end{bmatrix} , \; \boldsymbol{\theta}_4 = \begin{bmatrix} .21 \\ 0 \\ -.45 \end{bmatrix} \tag{31}$$

For this problem, $D_3, D_4 \subset D_2 \subset D_1$, and the domain $D = \bigcup_{j=1}^{4} D_j$ is partitioned as $D = \bigcup_{k=1}^{4} \Omega_k$, where

$$\Omega_1 = D_1 \setminus D_2,\ \Omega_2 = D_2 \setminus (D_3 \cup D_4),\ \Omega_3 = D_3,\ \Omega_4 = D_4\ . \quad (32)$$

The partitioned density $f_1(x, y)$ in the domain D is piecewise constant and given by

$$f_1 = \chi_{\Omega_{11}} + 0.2\chi_{\Omega_{12}} + 0.4\chi_{\Omega_{13}} + 0.4\chi_{\Omega_{14}}. \quad (33)$$

Suppose, furthermore, that 1028 uniformly spaced Fourier samples are taken, which corresponds to $1028/(128 \times 128) = 6.25\%$ of the Nyquist rate. Direct Fourier inversion (Figure 3(b)) exhibits strong aliasing artifacts. Suppose we know *a priori* that the image consists of four circles with *known* intensities. Then, the imaging problem can be formulated as the estimation of the center locations and the radii of each region, and the CRB for the unknown parameter vectors can be obtained using the techniques described in the previous section. The resulting CRB is a 12×12 matrix (12 parameters) and is rather difficult to interpret. We therefore do not show it explicitly.

We have applied the asymptotic global confidence region technique to the example of Figure 3(a) and computed the 95% asymptotic global confidence region for an example where the Fourier samples are corrupted with additive complex Gaussian noise at SNR=20. Figure 3(c) illustrates the resulting asymptotic global confidence region, in which asymptotically any unbiased estimate of the boundary will lie with 95% probability. This bound suggests that accurate estimates are possible even under at low sampling rates, if we have a priori knowledge of the number of domains and their densities. In addition, Figure 3(c) tells us that the estimates of small region boundaries are more uncertain, and boundaries nearer to the origin are harder to estimate.

VII. Conclusions

This paper has introduced a general method to compute Cramér-Rao bounds for parametric shape estimation in linear inverse problems, such as computed tomography, Fourier imaging, and deconvolution. We showed that if object boundaries are parameterized using a finite number of unknown parameters, Cramér-Rao bounds can be obtained using domain derivative techniques. In addition to providing explicit expressions for the components of the Cramér-Rao bounds for computed tomography, Fourier imaging, and deconvolution, our approach can be easily adapted to the particular form of any linear inverse problem with possibly nonlinear observations.

References

[1] C. K. Chui, *Multivariate Splines*. Philadelphia: SIAM, 1988.

[2] C. T. Zahn and R. Z. Roskies, "Fourier descriptors for plane closed curves," *IEEE Trans. on Computers*, pp. 269–281, March 1972.

[3] S. F. Yau and Y. Bresler, "Worst case Cramér-Rao bounds for parametric estimation of superimposed signals with applications," *IEEE Trans. on Signal Processing*, pp. 2973–2986, December 1992.

[4] D. J. Rossi and A. S. Willsky, "Reconstruction from projections based on detection and estimation of objects - Part I: Performance analysis," *IEEE Trans. on Acoustic Speech and Signal Processing*, pp. 886–897, August 1984.

[5] A. O. Hero, R. Piramuthu, J. A. Fessler, and S. R. Titus, "Minimax estimation computed tomography using high resolution anatomical side information and B-spline models," *IEEE Trans. on Information Theory*, pp. 920–938, April 1999.

[6] J. C. Ye, Y. Bresler, and P. Moulin, "Cramér-Rao bounds for 2-D target shape estimation in nonlinear inverse scattering problems with application to passive radar," *IEEE Trans. on Antennas and Propagat.*, pp. 771–783, May 2001.

[7] J. C. Ye, Y. Bresler, and P. Moulin, "Asymptotic global confidence regions in parametric shape estimation problems," *IEEE Trans. on Information Theory*, pp. 1881–1895, August 2000.

[8] K. M. Hanson, G. S. Gunningham, and R. J. McKee, "Uncertainty assessment for reconstructions based on deformable geometry," in *International Journal of Imaging Systems & Technology*, no. 6, pp. 506–512, 1997.

[9] H. L. VanTrees, *Detection, Estimation and Modulation Theory, Part I: Detection, Estimation, and Linear Modulation Theory*. New York: John Wiley & Sons, Inc., 1968.

[10] J. Sokolowski and J. Zolesio, *Introduction to Shape Optimization: Shape Sensitivity Analysis*. New York: Springer-Verlag, 1991.

[11] R. Venkataramani and Y. Bresler, "Perfect reconstruction formulas and bounds on aliasing error in sub-nyquist nonuniform sampling of multiband signals," *IEEE Trans. on Information Theory*, pp. 2173–2183, September 2000.

[12] "Metastatic bronchogenic carcinoma," in *http://www.med.harvard.edu/AANLIB/home.htm*.

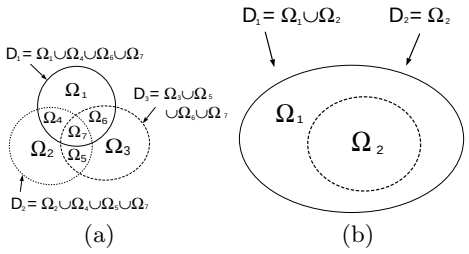

Fig. 1. Examples of disjoint partitions of sets.

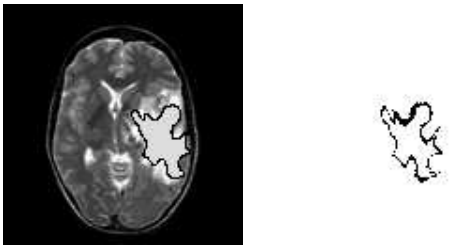

Fig. 2. (a) MRI scan of a human brain with tumor, (b) 98% global confidence region (indicated by the black region) for the boundary estimate using Fourier data corrupted by complex Gaussian additive noise at SNR=5.

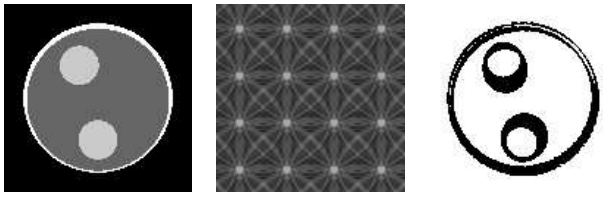

Fig. 3. (a) Synthetic phantom image; (b) direct Fourier inversion using 1028 uniformly spaced Fourier samples; (c) 95% global confidence regions from 1028 uniformly spaced Fourier samples with additive complex Gaussian noise at SNR=20.